Available online at www.sciencedirect.com
ScienceDirect
Trans. Nonferrous Met. Soc. China 33(2023) 3027−3038
Transactions of Nonferrous Metals Society of China
www.tnmsc.cn

Microstructure and mechanical properties of ultrasonic welded copper to aluminum cables joints

Xian-ming CHENG[1], Ke YANG[2], Si-zhan LIU[1], Shan-lin JI[1], Jian WANG[1]

1. College of Mechanical and Electrical Engineering, Hohai University, Changzhou 213022, China;
2. College of Materials Science and Engineering, Hohai University, Changzhou 213022, China

Received 31 March 2022; accepted 1 June 2022

Abstract: The experiments of ultrasonic welding were carried out for BVR2.0 copper (Cu) cables and BLV6.0 aluminum (Al) cables with different welding parameters. Scanning electron microscopy (SEM), energy dispersive spectroscopy (EDS), temperature measurement, microhardness evaluation and tensile tests were conducted to investigate the microstructure and mechanical properties of Cu−Al cables joints. The results show that the tensile load of Cu−Al joints reaches 355.6 N, while the welding parameters are set as follows: welding pressure of 0.21 MPa, amplitude of 31%, and time of 860 ms. The diffusion thickness of well-welded Cu−Al joint is only about 3 μm and the peak temperature is 212 °C, which avoids the formation of intermetallic (IMC) effectively. The joint fractures on the copper side rather than the interface of the Cu−Al with a ductile−brittle hybrid fracture mode, indicating that the joint has excellent properties.

Key words: ultrasonic welding; welding parameters; Cu−Al cables joints; microstructure; mechanical properties

1 Introduction

Dissimilar metal joints of copper (Cu) and aluminium (Al) alloys are used extensively in automotive and electronics industries to achieve the goals of reducing weight and cost [1]. Cu has been identified as an excellent material of cable for its high electrical and thermal conductivity, as well as corrosion resistance performances, making its wide application in electronics, electric power, new energy vehicles, aerospace and other fields [2−5]. However, the reserves of Cu resources are scarce (only 0.01% in the earth's crust) and the price is high. Meanwhile, Al and its alloys have low density (only 1/3 of copper), high electrical conductivity, rich reserves (8% in the crust) and low cost. Unfortunately, Al also has some disadvantages, such as poor corrosion resistance and oxide layer, resulting in large contact resistance at the joint [6]. Thus, dissimilar material joints between Cu and Al are inevitable. Since joints of Cu−Al can not only combine the advantages of the two materials to meet the application requirements [7,8], but also promote the development of product lightweight component [9]. Dissimilar material joining has become an unavoidable development trend [10−13], such as the connection of Cu−Al foils [10], battery electrodes, tabs and charging pile of electric vehicle battery. In order to reduce weight and cost, Al cables are used for internal circuit connection of battery, while Cu cables are used for high-voltage harness. Therefore, the joints of Cu−Al cables are generally used for current confluence or shunt. However, due to the huge differences in melting temperature, thermal conductivity, and tensile strength, joining Al to Cu is an enormous challenge, resulting in the formation of brittle intermetallic compounds (IMCs).

Ultrasonic welding (USW) obtains increasing

Corresponding author: Ke YANG, Tel: +86-519-85192035, E-mail: yangke_hhuc@126.com
DOI: 10.1016/S1003-6326(23)66315-0

popularity in dissimilar metal joints as it has the advantages of high welding speed, high welding strength, low cost and good conductivity of joints. During a typical USW process, clamping force and high-frequency ultrasonic vibration are used to produce plastic deformation and mechanical fitting, and the base metal does not melt. Therefore, it is a solid-phase connection technology [14]. In recent years, a large number of investigations have been carried out on the ultrasonic welding process of Cu−Al to study the welding mechanism. SATPATHI and SAHOO [15] reported that the surface condition of sheets and welding time could affect the joint quality, and the quality is enhanced with the increase of welding time. Further, they studied the interfacial temperature rise with welding time [16,17], and suggested that the hardness of the connecting interface was improved and intermetallic (IMC) layer was produced. LIU et al [18] carried out the USW experiment of 0.8 mm-thick Cu and Al sheets. The research showed that the welding amplitude had an effect on the IMC layer, and the additional heat source could promote the welding process. LI et al [19] observed that with the increase in welding pressure, the thickness of IMC layer first increased and then decreased. In addition, they established a finite element model to simulate the process of weld temperature and plastic deformation with different welding time [20], and then verified the accuracy of the model through experiments. DHARA and DAS [10] studied the effects of welding process on the properties of joint, including its mechanical properties, microhardness and microstructure. But they used the single variable method in the experiment, only considering the effect of a single process parameter on the joint performance, and did not take the influence of the interaction among the process parameters into account. Based on the reviewed literature, there is a lot of research on the USW of Cu−Al sheets, but the mechanical properties of Cu−Al wires have not been reported.

This work was to identify the parametric interdependencies and obtain a good performance of the USW joint, including tensile properties, microhardness and fracture mode. Additionally, the micro morphology, peak temperature and interface composition of the joints were also studied. The joining mechanisms of the Cu−Al joints were thoroughly discussed.

2 Experimental

2.1 Experimental materials and equipment

In this study, single core Cu and Al cables were conducted in the experiment, which were multi-strand with a nominal cross section of 2.5 mm^2 (BVR2.5) and single-strand with a nominal cross section of 6 mm^2 (BLV6), respectively. The Cu cables consisted of nineteen-strands of Cu strand conductors with 0.41 mm in diameter, and the Al cables were made up of one-strand of Al core with 2.7 mm in diameter. Both of them were cut off with a length of 100 mm. The insulating material was stripped to expose the core material with a length of 18 mm according to USCAR−45 standard, as shown in Fig. 1(a).

CJH−1600 machine was utilized for the USW, as presented in Fig. 2. This machine was capable of delivering a power rating of 3 kW and operating at 20 kHz. The welded joint was obtained by placing the Cu cable on the bottom and the Al cable on the

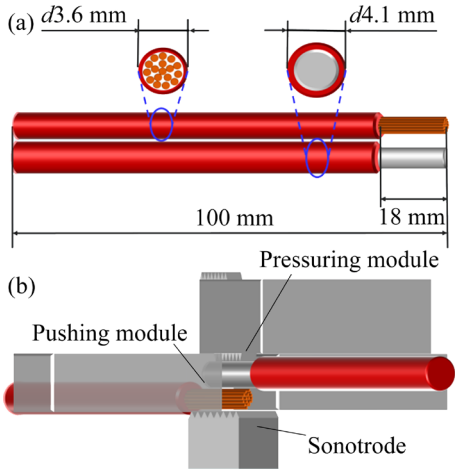

Fig. 1 Dimensions of test specimen (a) and schematic representation of welding sample placement (b)

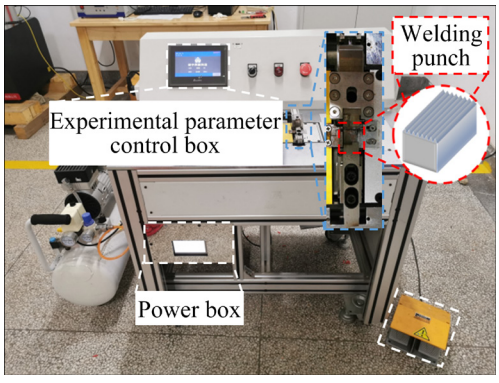

Fig. 2 Ultrasonic welding test equipment

top, as demonstrated in Fig. 1(b).

The welding process consisted of four steps, as shown in Fig. 3. Step 1: The pushing model clamps the cables laterally with the pre-pressure P_0, which reduces the gap between Cu and Al cables and limits the transverse movement of the wires. Then, the pressuring model moves laterally close to the pushing model. Step 2: The pressuring model comes down to provide the welding pressure P_1. Step 3: The sonotrode A vibrates at high frequency to provide welding energy, and the cables are combined under the action of ultrasonic vibration. Step 4: The pressuring model moves upwards and retracts to complete the welding.

To assess the tensile strength of the joint, tensile tests were carried out by using a UTM5105 electronic universal testing machine at a pulling speed of 20 mm/min. The tensile fractograph and microstructures were observed by scanning electron microscope (SEM). The chemical compositions of the cross sections were characterized via an energy dispersive spectroscopy (EDS). During welding, the K-type thermocouples were clamped between Cu and Al wires, and the peak temperature data at the interface were recorded by a UT−325 digital thermometer. The Vickers hardness of the weld joints was measured by HVS−1000A Vickers hardness tester with a load of 50 g and a dwell time of 15 s. The interval of measuring points was 50 μm, which was selected from Al to Cu and along with the connection interface.

2.2 Experimental design

Response surface method (RSM), as a statistical optimization method, has been widely used in the fields of biopharmaceutical, material science and non-ferrous metal smelting. In this method, the regression method was used to establish the relationship between the experimental factors and the response values, which can evaluate the factors and the interaction relationship between the factors, and further determine the optimal level of each factor to make the response value excellent. Box Behnken design (BBD) can not set all experimental parameters at a high level at the same time, which can avoid damage to the horn caused by excessive welding process parameters and reduce the number of experiments. In the present work, RSM based on BBD was scheduled to establish the relationship between ultrasonic welding process parameters and joint tensile strength, so as to optimize the welding process parameters and investigate the influence of welding process parameters and their interaction on joints.

When considering that the ultrasonic metal welding is a highly nonlinear system, a quadratic polynomial regression model was used to predict the tensile strength of joints with different process parameters [21]:

$$Y = b_0 + \sum_{i=1}^{n} b_i X_i + \sum_{i=1}^{n} b_{ii} X_i^2 + \sum_{i=1}^{n} \sum_{j=i+1}^{n} b_{ij} X_i X_j \quad (1)$$

where Y denotes the dependent response variable

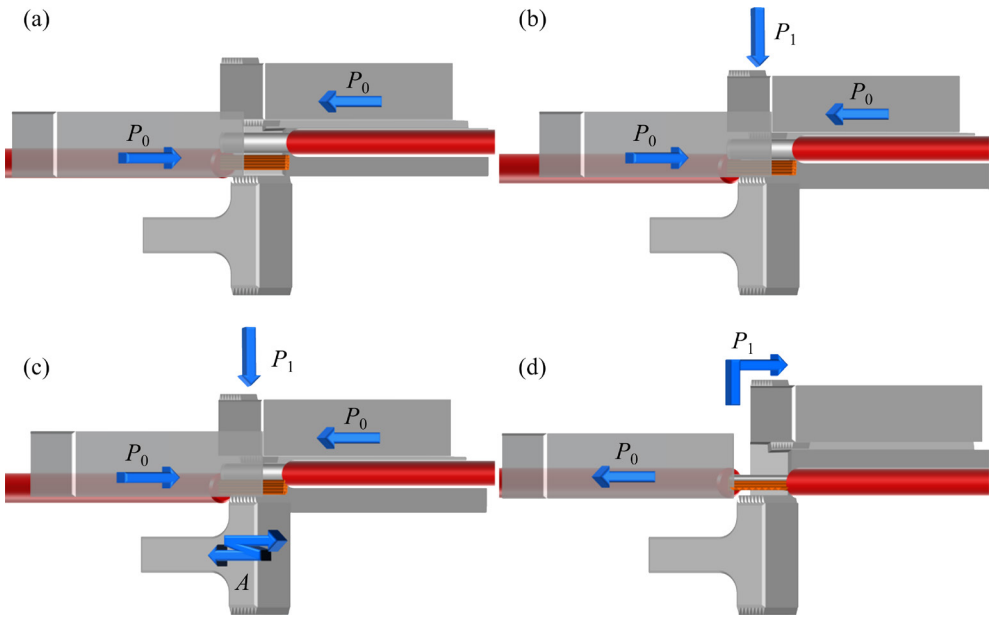

Fig. 3 Processing steps during ultrasonic welding of cables: (a) Step 1; (b) Step 2; (c) Step 3; (d) Step 4

(i.e., tensile strength), b_0 is a constant term, b_i, b_{ii} and b_{ij} are the linear, quadratic and interactive coefficients, respectively [22], X_i and X_j represent the independent variables, and n is the number of these factors. The independent variables, such as welding pressure (X_1), welding amplitude (X_2) and welding time (X_3), were chosen in these experiments according to the previous research results. The coding of factor level in this model is given in Table 1 with each factor set at its high level (+1), low level (−1) and medium level (0).

Table 1 Coding of experimental factors and levels

Parameter	Code	Level		
		−1	0	+1
Welding pressure/MPa	X_1	0.20	0.25	0.30
Welding amplitude/%	X_2	25	30	35
Welding time/ms	X_3	800	1000	1200

Analysis of variance (ANOVA) was used to estimate the influence level and significance of linear, quadratic and interaction between variables within 95% confidence interval. Then, the model was used to predict the tensile results of the joint. Finally, the factor level with the highest tensile strength of the joint was predicted by the model and verified by experiments.

3 Results and discussion

3.1 Model fitting

A total of 17 groups of test schemes with 3 input parameters and 3 levels, according to the principle of RSM, were designed by using the Design Expert Software. The experimental results are given in Table 2, and the tensile load response range is from 107.40 to 330.67 N.

Based on the estimated values of the regression coefficients in Table 2, a second-order polynomial regression model can be rewritten as

$$F=-4185.77+12288.32X_1+125.85X_2+2.95X_3-169.07X_1X_2+0.68X_1X_3-0.04X_2X_3-18168.8X_1^2-0.86X_2^2-0.001X_3^2 \quad (2)$$

Table 3 gives the ANOVA results of the quadratic polynomial regression model. The terms of model are significant as it is less than 0.05. The p-value of the model is less than 0.001, which indicates that the model is of great significance

Table 2 Box Behnken experimental design matrix and results

Run No.	Factor			Tensile load/N
	X_1/MPa	X_2/%	X_3/ms	
1	0.25	35	800	304.20
2	0.25	30	1000	327.00
3	0.30	30	800	210.73
4	0.25	25	1200	309.07
5	0.25	30	1000	346.00
6	0.30	25	1000	290.87
7	0.20	30	1200	258.53
8	0.20	25	1000	330.67
9	0.25	35	1200	135.40
10	0.30	35	1000	107.40
11	0.25	30	1000	317.20
12	0.25	25	800	312.60
13	0.25	30	1000	321.20
14	0.30	30	1200	159.60
15	0.20	35	1000	316.27
16	0.25	30	1000	330.07
17	0.20	30	800	337.00

Table 3 Analysis of variance for response surface quadratic model

Source	Sum of squares	df	Mean square	F value	p-value
Model	91406.72	9	10156.30	86.70	< 0.001
X_1	28069.10	1	28069.10	239.61	< 0.001
X_2	18044.30	1	18044.30	154.03	< 0.001
X_3	11395.22	1	11395.20	97.27	< 0.001
X_1X_2	7146.17	1	7146.17	61.00	0.001
X_1X_3	186.87	1	186.87	1.60	0.247
X_2X_3	6828.54	1	6828.54	58.29	0.001
X_1^2	8686.98	1	8686.98	74.15	< 0.001
X_2^2	1958.92	1	1958.92	16.72	0.004
X_3^2	7219.11	1	7219.11	61.62	0.001
Lack of fit	328.29	3	109.43	0.89	0.518
Std. dev.	10.82		R^2		0.991
Mean	277.28		Adj R^2		0.979
C.V./%	3.90		Pred R^2		0.934
PRESS	6021		Ade precision		28.064

and there is an obvious second order regression relationship between welding process parameters and joint tensile strength [23]. In this model, except for the interaction term of X_1X_3, the other primary terms, secondary terms and interaction terms have a great significant impact on the tensile load of the joint. The F-value determines the importance of the factor. Thus, the significant influence of various factors and their interaction on the joint strength is $X_1 > X_2 > X_3 > X_1X_2 > X_2X_3$. The coefficient of determination R^2 determines the goodness of fit of the model to the data. Therefore, 99.11% of the variability in new experimental data is able to explain. The value of the adjusted R^2 (Adjusted R^2=0.979) is also large enough to support the high significance of the model.

Figure 4 shows the normal probability distribution of residual tensile load. In Fig. 4, 17 groups of residual data points are basically distributed along the straight line in the normal probability graph of residual, indicating that the residual belongs to normal distribution.

The comparison between the predicted value of the model and the actual value is presented in Fig. 5. The actual values are evenly distributed on both sides of the standard line, and the maximum error is no more than 17 N, indicating that the model can accurately describe the relationship between joint tensile load and welding process.

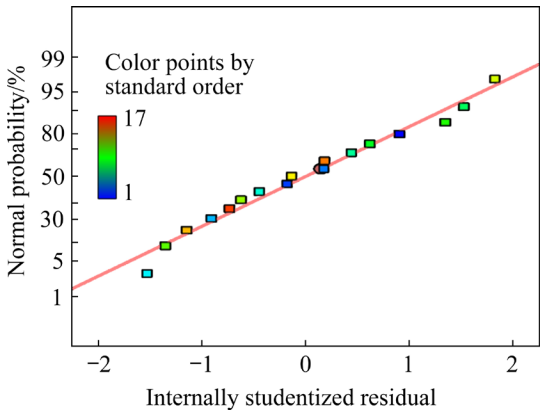

Fig. 4 Normal probability plot of residuals for tensile load of RSM model

3.2 Analysis of RSM for tensile strength

In order to visually express the interaction influence among various factors, according to the prediction model obtained from Eq. (2), the estimated response surface and contour plot for welding pressure, amplitude, time and tensile load are reflected in Fig. 6. The influence level of the factors is determined by the slope of the response surface, and the significance of the interaction is determined by the contour curvature.

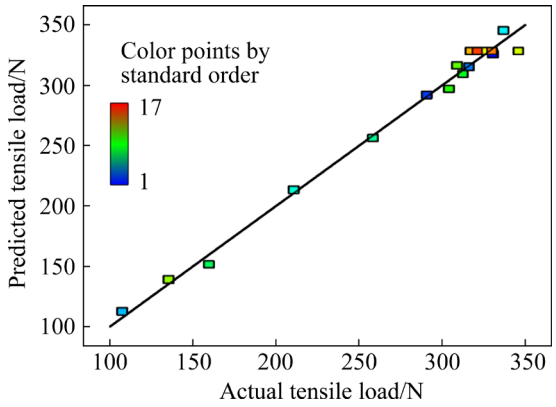

Fig. 5 Correlation between actual and predicted tensile load

Figures 6(a, b) show the influence of the interaction between welding pressure and amplitude when the welding time is 940 ms. As can be seen from Fig. 6(a), the tensile load of the joint increases with the increase in welding pressure and amplitude within a certain range. Besides, the surface of welding pressure is steeper than that of amplitude, indicating that the influence of welding pressure is more significant than that of amplitude. In Fig. 6(b), the curvature of the contour line is large, indicating that the interaction between welding pressure and amplitude is significant. In addition, the welding pressure and amplitude promote the plastic deformation of the material at the same time. If the welding amplitude is 25% and the pressure increases from 0.2 to 0.24 MPa, the tensile load of the joint increases from 323 to 351.1 N. When the welding pressure is 0.2 MPa, the oxide layer on the wire surface is not completely broken, and the mutual diffusion of atoms is hindered, which is not conducive to the formation of weld. The tensile load of the joint increases significantly with the increase of welding pressure to 0.24 MPa. Because tensile load expands the contact area of the cables and strengthens the friction of the contact surface to produce large plastic deformation, the oxide layer is completely broken to form mechanical fitting.

Similarly, when the welding pressure is set to be 0.2 MPa, the welding time is 940 ms, and the welding amplitude increases from 25% to 31%, the tensile load of the joint increases from 323 to

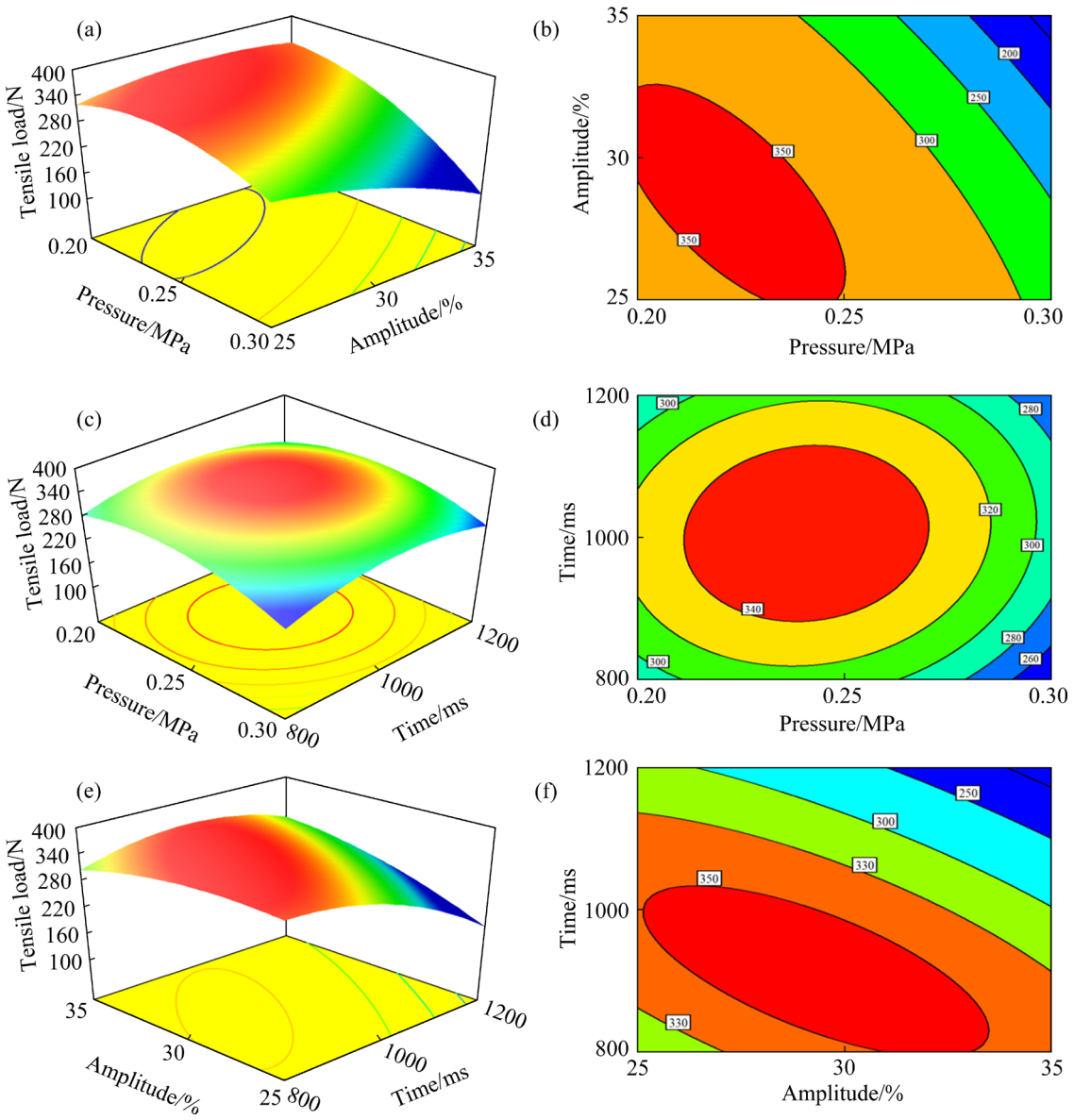

Fig. 6 Response surface and contour plots for weld strength: (a) X_1−X_2 response surface; (b) X_1−X_2 contour plot; (c) X_1−X_3 response surface; (d) X_1−X_3 contour plot; (e) X_2−X_3 response surface; (f) X_2−X_3 contour plot

352.3 N. The increase of amplitude makes the dislocation of wire plastic flow evolve to the trend conducive to plastic flow. Therefore, the plasticity of the conductor is improved and it is easier to form mechanical embedded solder joints. On the other hand, welding amplitude also affects the mechanical fitting depth between metals. If the welding pressure exceeds 0.24 MPa or amplitude exceeds 31%, the joint strength decreases. The reason for this behavior is that too much welding pressure or amplitude greatly reduces the radial cross-sectional area of the joint. It can be inferred that there is an interactive region between welding pressure and amplitude, which makes the joint bonding effect optimal.

Figures 6(c, d) show the influence of the interaction between pressure and time when the welding amplitude is 25%. Figures 6(e, f) show the influence of the interaction between time and amplitude when the welding pressure is 0.22 MPa. It can be seen from Figs. 6(c−f) that the influence of welding time on joint strength also increases first and then decreases, and the influence degree is less than the welding amplitude. When the welding pressure is 0.22 MPa and the welding time increases from 800 to 1000 ms, the tensile load increases from 307 to 344.9 N. As welding time gets longer, the welding energy is increased, which

is helpful in removing the oxide layer on the surface of Al, so as to make the metal atoms between Cu−Al close to each other and realize mechanical fitting. However, too long welding time increases the input energy and temperature of the joint. Severe deformation occurs on the Al side, the effective cross-sectional area of the joint decreases, and high stress concentration occurs at the edge of the nugget on the Al side. Under this condition, brittle fracture is easy to occur on the Al side and the tensile strength is reduced. Figure 6(d) shows that the interaction between welding pressure and time is not obvious, while Fig. 6(f) shows that the interaction between welding time and amplitude is significant. This indicates that there is an interactive region between welding time and amplitude, which makes the tensile performance of the joint the highest.

To sum up, welding pressure is the most critical parameter for improving the tensile strength of the joint, followed by welding amplitude and time. The interaction between welding pressure and amplitude, as well as welding time and amplitude, is significant, which is consistent with the results of ANOVA.

3.3 Verification of optimum welding parameters

The tensile load was set as the desired target to predict the maximum tensile strength of the joint. The factors and range were set as welding pressure of 0.2−0.3 MPa, welding amplitude of 25%−35% and welding time of 800−1200 ms.

Design Expert 8.0 software was used for the sake of getting the global optimal parameters, and the number of starting points of simplex optimization search was set to be 30. The conditions for obtaining the maximum tensile strength are as follows: welding pressure 0.21 MPa, welding amplitude 31.39%, welding time 858.55 ms, and the maximum tensile load of the joint is 359.132 N. Considering the accuracy of equipment parameters, the above parameters are adjusted, and the results are given in Table 4.

Figure 7 shows the tensile load−displacement curve of the joint. The peak load is 355.6 N, which is much higher than the maximum value of 337 N in Table 2. The difference between the optimal and the prediction result is only 0.8%, which also indicates the goodness of fit of the mathematical model in this study. It can be seen that the joint reaches the elastic limit at 300 N, followed by the plastic deformation region, indicating that it has good toughness.

From Fig. 7, it can also be seen that there is still a small plastic deformation area after the joint is broken. This is because the tensile load at the joint is greater than that of a single-strand of Cu conductor. Due to the uneven stress on each Cu conductor during welding [24], partial Cu wires are pulled off after large displacement. MOSTAFAVI and MARKERT [25] suggest that the bonding condition can vary at different interfaces and bonded areas of different strengths are developed.

3.4 Analysis of joint microstructure

The interaction mechanism of ultrasonic welding can be further explored through the analysis of interface micro morphology. Figure 8 shows the SEM images of the Cu−Al wires bonding interface with different welding parameters. The bonding interface morphology of Experiment No. 8 (welding pressure of 0.2 MPa, amplitude of 25%, and time of 1000 ms) is shown in Fig. 8(a). As can be seen from the trend of weld formation that the weld is formed first along the direction of welding pressure because the welding pressure and amplitude jointly promote the plastic flow of the material. On the other hand, only part of the Cu−Al cables is connected due to the plastic deformation ability of the material being weak under the condition of low welding pressure and amplitude. The Cu−Al interface is in a “stick-slip” state, and the plastic flow on the Al side does not fill the cavity generated by ultrasonic vibration in time [26]. This condition is considered as under-welded.

Figures 8(b, c) show the bonding interface

Table 4 Adjustment of optimal welding process parameters

Condition	Frequency/Hz	Welding pressure/MPa	Welding amplitude/%	Welding time/ms	Tensile load/N
Optimum	2.0×10^4	0.21	31.39	858.55	359.132
Modified	2.0×10^4	0.21	31	860	358.754

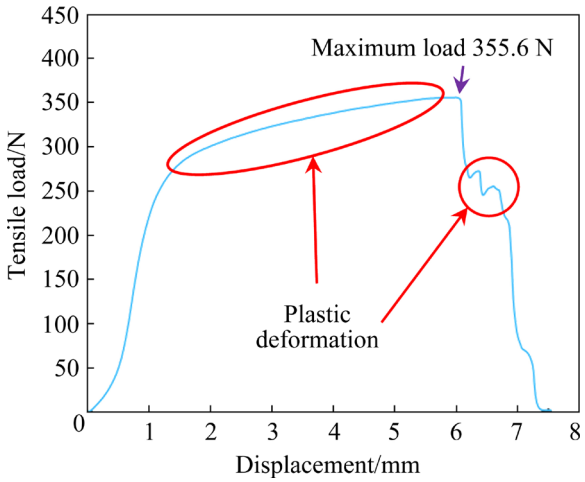

Fig. 7 Tensile load−displacement curve of soldered joint

morphologies under the optimal welding parameters and Experiment No. 3 (the welding pressure of 0.3 MPa, amplitude of 30%, and time of 800 ms). As can be seen from Fig. 8 that the Cu−Al interface is well bonded and no obvious IMC is formed when the amplitude is larger than 30%. Compared with Experiment No. 8, the welding time under the optimal welding parameters is shorter, indicating that the amplitude is more conducive to promoting the plastic flow of materials than the welding time. However, when the welding pressure and amplitude increase, the joint becomes over-welded.

3.5 Analysis of interface element

According to the results of micro morphology analysis, the joint is divided into three types: under-welded (welding pressure of 0.2 MPa, amplitude of 25%, and time of 1000 ms), well-welded (the optimal welding parameters) and over-welded (welding pressure of 0.3 MPa, amplitude of 30%, and time of 800 ms). In order to investigate the element composition of Cu−Al interface under different welding parameters, EDS line scanning was used at the line drawn in Fig. 8.

The EDS line analysis results in three cases are shown in Fig. 9, indicating that Cu and Al diffuse to each other. The diffusion process is stable and continuous, and there is no platform transition region, illustrating that there is no IMC formed. By comparing Figs. 9(a, b, c), it can be found that increasing the welding amplitude and pressure can significantly improve the thickness of atomic diffusion layer. In addition, the atomic diffusion distance is very short, and the diffusion thickness is

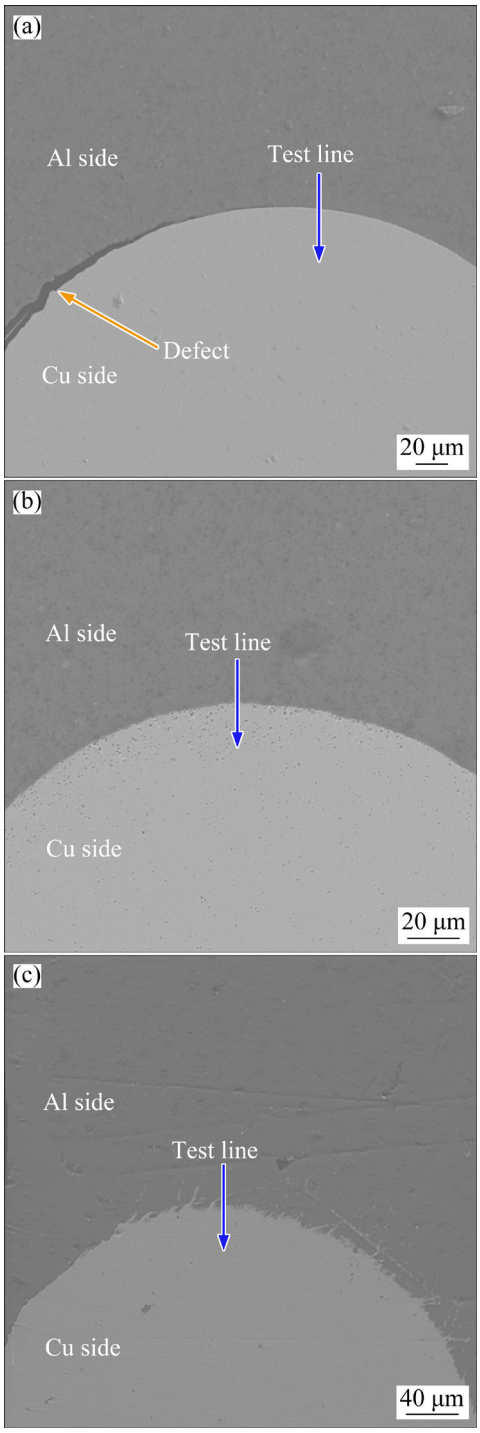

Fig. 8 SEM images of weld interface: (a) Welding pressure of 0.2 MPa, amplitude of 25%, and time of 1000 ms; (b) Optimal welding parameters; (c) Welding pressure of 0.3 MPa, amplitude of 30%, and time of 800 ms

3 μm under the optimal parameters. This is because the USW process has short welding time and low welding peak temperature, which is not enough to drive the reaction interface to form IMC.

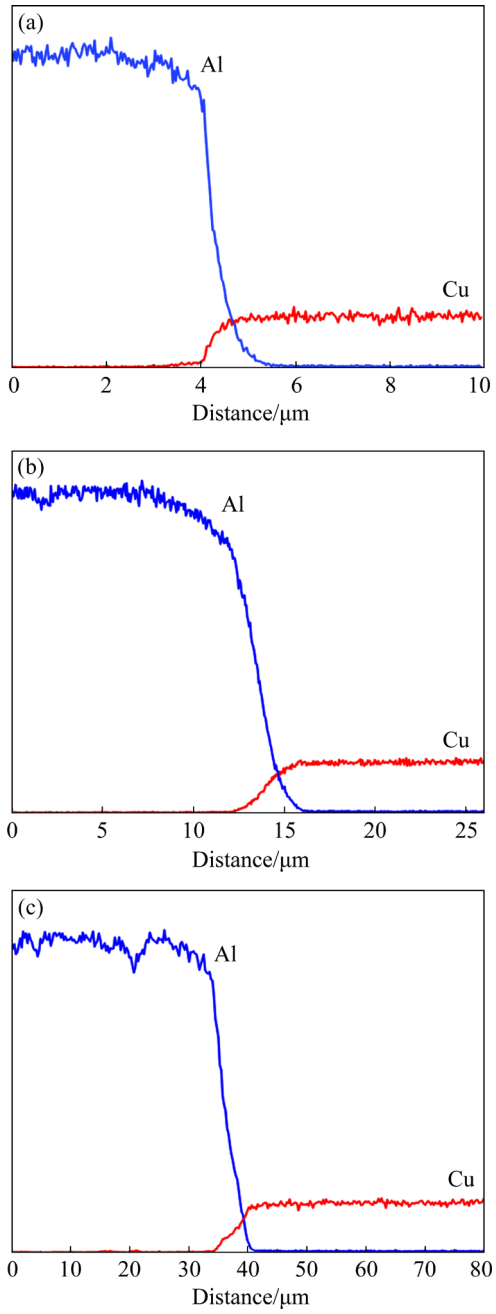

Fig. 9 Results of EDS line scan analysis of joints: (a) Under-weld; (b) Well-welded; (c) Over-welded

3.6 Analysis of peak temperature

In order to further study the influence of welding parameters and their interaction on interface diffusion behavior, the interface temperature of the joint was analyzed. Figure 10 shows the peak temperature curve measured under different welding parameters. The temperature does not change significantly about 500 ms before welding because the ultrasonic vibration is not released. When the piezoelectric ceramic drives the sound pole to produce ultrasonic vibration, the welding temperature increases rapidly with the increase of welding time, and then the temperature rise speed decreases. The temperature reaches the peak value when the set welding time is reached, and then decreases gradually.

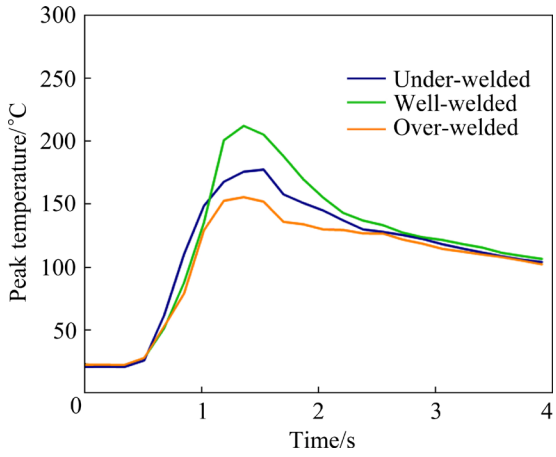

Fig. 10 Peak temperatures of interface with different welding parameters

The weld thermal cycles show that at the initial stage of welding, a large amount of friction heat and plastic deformation heat are generated at the contact interface due to high-frequency vibration [17]. With the increase of welding area, the amplitude decreases gradually under the pressure, and the rate of interfacial heat generation decreases. Under over-welded condition, the peak temperature at Cu−Al interface is only 155.6 °C, while the peak temperature increases to 212.2 °C under the optimal welding parameters. The peak temperature at the interface is much lower than the metal melting point of the base metal, which indicates that ultrasonic welding is a solid-state connection. By comparing the temperature results of well-welded and over-welded conditions, it is found that the peak temperature of over-welded interface is lower, which indicates that excessive welding pressure hinders the amplitude movement rather than increases the interface temperature. By comparing the results of well-welded and under-welded conditions, it is found that the welding amplitude has a more significant effect on the interface temperature rise than the welding time. Therefore, the welding time and amplitude determine the peak temperature of the interface.

3.7 Analysis of microhardness

Figure 11 illustrates microhardness distribution

curve of the joint under the optimal parameters. It can be seen that the hardness increases gradually from Al to Cu, and the value is in the range of HV 26−83. From the transverse hardness distribution diagram, it can be seen that the transverse hardness value fluctuates greatly between HV 38 and HV 68, which is higher than that on the Al but lower than that on the Cu. This is because the stress at the interface between Cu and Al is uneven and the atomic diffusion velocity is different. The hardness at the interface is lower than that of Cu, indicating that the brittle and hard IMCs are not formed and the joint bonds effectively.

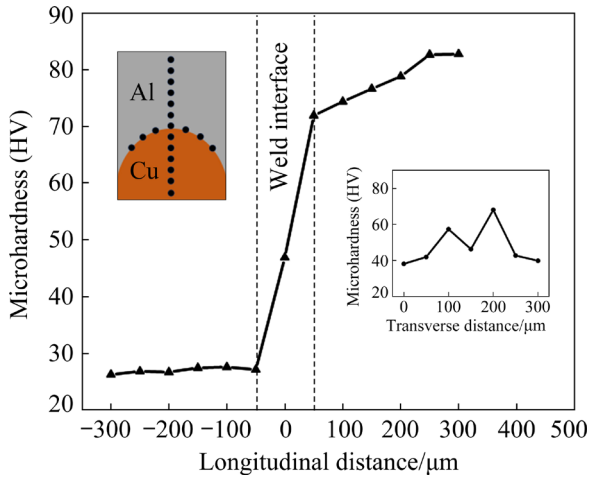

Fig. 11 Microhardness of welding joint

3.8 Analysis of fracture

Figure 12(a) shows the fracture morphology of under-welded joint. The fracture occurs at the junction of Cu−Al interface due to the low welding process parameters. This suggests that only the local mechanical fitting between the interfaces is formed under the interaction of ultrasonic vibration and pressure because the oxide layer on the Al surface is not completely broken. During stretching, only part of the oxide layer on the Al surface falls off with shear stress. Figure 12(b) depicts the fracture morphology of well-welded joint. The joint breaks on the Cu side. This is because under the interaction of static pressure and large amplitude, the Cu−Al interface is bonded well, and the bonding strength is higher than the tensile strength of single strand Cu wire. During the process of tensile loading, the Cu wire is plastically deformed and breaks when it reaches the yield strength limit. Dimple, tearing ridges and cleavage planes are found on the fracture surface, indicating that it is a ductile−brittle hybrid fracture. Figures 12(c) shows the fracture morphology of over-welded joint. The fracture occurs on the Al side because it has severe plastic deformation and the effective bearing area is reduced under excessive welding pressure. There are only a few dimples in the fracture morphology, illustrating that the toughness of the joint is poor with these parameters.

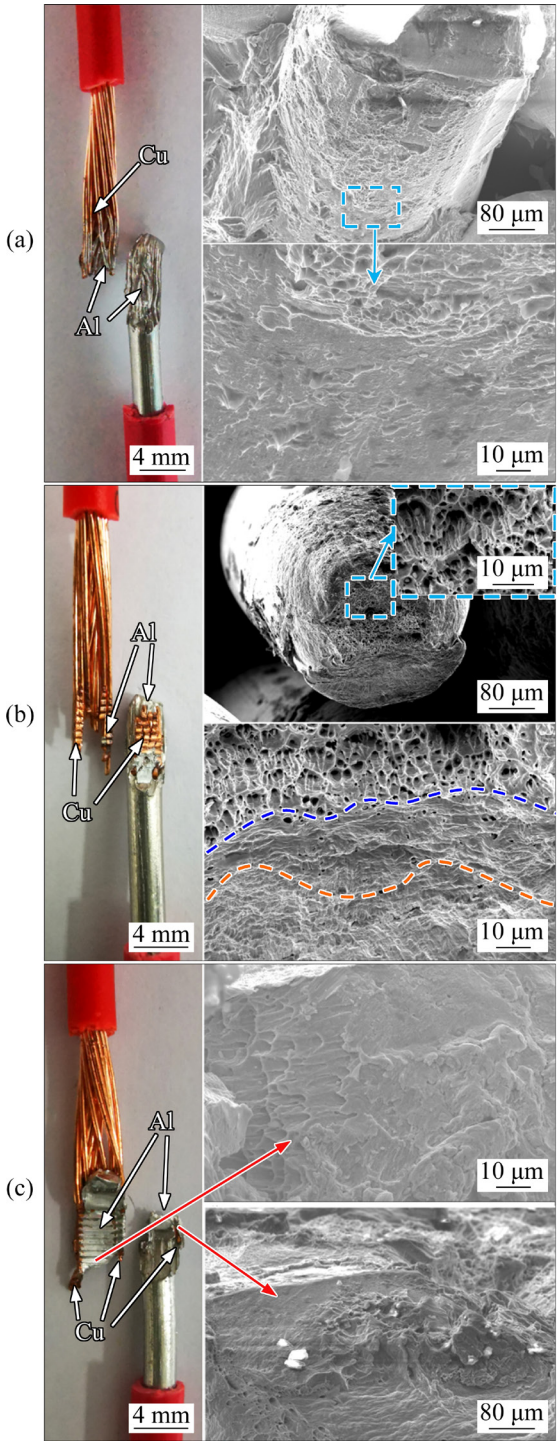

Fig. 12 Morphologies of tensile fracture samples: (a) Under-welded; (b) Well-welded; (c) Over-welded

4 Conclusions

(1) According to the RSM, the optimum welding parameters are obtained as follows: welding pressure 0.21 MPa, amplitude 31% and time 860 ms, and the peak tensile load reaches 355.6 N.

(2) The mutual diffusion thickness of Cu−Al is about 3 μm, which avoids the formation of IMC at the interface, indicating that the connection is mainly realized by mechanical fitting. The maximum welding temperature of the interface is 212.2 °C, which is lower than the melting point of the base metal, representing that USW is solid-phase connection.

(3) With the optimal parameters, the bonding strength of the joint is higher than the tensile load of single strand Cu wire, and the fracture occurs on the Cu side with a ductile−brittle hybrid fracture mode, indicating that the joint has excellent properties.

Acknowledgments

This work was financially supported by the National Key Research and Development Program of China (No. 2017YFE0100100), the Changzhou Key Research and Development Plan, China (No. CE20205046) and the Fundamental Research Funds for the Central Universities of China (No. B220203019).

References

[1] AO S S, LI C J, ZHANG W, WU M P, DAI Y, CHEN Y, LUO Z. Microstructure evolution and mechanical properties of Al/Cu ultrasonic spot welded joints during thermal processing [J]. Journal of Manufacturing Processes, 2019, 41: 307−314.

[2] JIANG Yan-bin, LI Yong-shuai, LEI Yu, XIE Jian-xin. Cross-sectional structure, microstructure and mechanical property evolutions of brass cladding pure copper stranded wire composite during drawing [J]. Transactions of Nonferrous Metals Society of China, 2020, 30(7): 1857−1872.

[3] NI Z L, YANG J J, GAO Z T, HAO Y X, CHEN L F, YE F X. Joint formation in ultrasonic spot welding of aluminum to copper and the effect of particle interlayer [J]. Journal of Manufacturing Processes, 2020, 50(4): 57−67.

[4] RAJ N M, KUMARASWAMIDHAS L A, VENDAN S A. Experimental studies and finite element simulation of ultrasonic welding of Cu alloy [J]. Bulletin of the Polish Academy of Sciences−Technical Sciences, 2016, 64(3): 535−546.

[5] LI Y L, CHU Z H, LI X W, PAN Y L, YAMAGUCHI T, WANG W Q. Swirl-like Cu−Sn phase formation and the effects on the ultrasonic spot welded joint of Sn-coated Cu plates [J]. Journal of Materials Processing Technology, 2021, 288(4): 116911.

[6] MOSTAFAVI S, HESSER D F, MARKERT B. Effect of process parameters on the interface temperature in ultrasonic aluminum wire bonding [J]. Journal of Manufacturing Processes, 2018, 36(3): 104−114.

[7] MEHTA K P, BADHEKA VISHVESH J. Influence of tool pin design on properties of dissimilar copper to aluminum friction stir welding [J]. Transactions of Nonferrous Metals Society of China, 2017, 27(1): 36−54.

[8] ARGESI F B, SHAMSIPUR A, MIRSALEHI S E. Preparation of bimetallic nano-composite by dissimilar friction stir welding of copper to aluminum alloy [J]. Transactions of Nonferrous Metals Society of China, 2021, 31(5): 1363−1380.

[9] VICTOR CHRISTY J, ISMAIL MOURAD A H, SHERIF M M, SHIVAMURTHY B. Review of recent trends in friction stir welding process of aluminum alloys and aluminum metal matrix composites [J]. Transactions of Nonferrous Metals Society of China, 2021, 31(11): 3281−3309.

[10] DHARA S, DAS A. Impact of ultrasonic welding on multi-layered Al−Cu joint for electric vehicle battery applications: A layer-wise microstructural analysis [J]. Materials Science and Engineering A, 2020, 791: 139795.

[11] ZHANG Z J, WANG K F, LI J J, YU Q, CAI W N. Investigation of interfacial layer for ultrasonic spot welded aluminum to copper joints [J]. Scientific Reports, 2017, 7(1): 12505.

[12] SHIN H S, LEON D M. Mechanical performance and electrical resistance of ultrasonic welded multiple Cu−Al layers [J]. Journal of Materials Processing Technology, 2017, 241: 141−153.

[13] FUJII H T, ENDO H, SAT Y S, KOKAWA H. Interfacial microstructure evolution and weld formation during ultrasonic welding of Al alloy to Cu [J]. Materials Characterization, 2018, 139: 233−240.

[14] KUMAR S, WU C S, PADHY G K, DING W. Application of ultrasonic vibrations in welding and metal processing: A status review [J]. Journal of Manufacturing Processes, 2017, 26: 295−322.

[15] SATPATHY M P, SAHOO S K. Microstructural and mechanical performance of ultrasonic spot welded Al−Cu joints for various surface conditions [J]. Journal of Manufacturing Processes, 2016, 22: 108−114.

[16] SATPATHY M P, SAHOO S K. Mechanical performance and metallurgical characterization of ultrasonically welded dissimilar joints [J]. Journal of Manufacturing Processes, 2017, 25: 443−451.

[17] SATPATHY M P, MISHRA S B, SAHOO S K. Ultrasonic spot welding of aluminum-copper dissimilar metals: A study on joint strength by experimentation and machine learning techniques [J]. Journal of Manufacturing Processes, 2018, 33: 96−110.

[18] LIU J, CAO B, YANG J W. Modelling intermetallic phase

growth during high-power ultrasonic welding of copper and aluminum [J]. Journal of Manufacturing Processes, 2018, 35: 595−603.
[19] LI H, CAO B, YANG J W, LIU J. Modeling of resistance heat assisted ultrasonic welding of Cu−Al joint [J]. Journal of Materials Processing Technology, 2017, 256: 121−131.
[20] LI H, CAO B. Effects of welding pressure on high-power ultrasonic spot welding of Cu/Al dissimilar metals [J]. Journal of Manufacturing Processes, 2019, 46: 194−203.
[21] ELANGOVAN S, ANAND K, PRAKASAN K. Parametric optimization of ultrasonic metal welding using response surface methodology and genetic algorithm [J]. International Journal of Advanced Manufacturing Technology, 2012, 63(5): 561−572.
[22] GANESAMOORTHI B, KALAIVANAN S, DINESH R, KUMAR T N, ANAND K. Optimization technique using response surface method for USMW process [J]. Procedia Social and Behavioral Sciences, 2015, 189: 169−174.
[23] PRADEEP K J. Effect of process parameter characteristics on joint strength during ultrasonic metal welding of electrical contacts [J]. Welding in the World, 2020, 64(1): 73−82.
[24] CHENG Xian-ming, YANG Ke, LIU Si-zhan, JI Shan-lin, WANG Jian. Effect of ultrasonic welding process parameters on properties of copper conductor joint [J]. The Chinese Journal of Nonferrous Metals, 2022, 32(11): 3341−3351. (in Chinese).
[25] MOSTAFAVI S, MARKERT B. Ultrasonic weld strength and weld microstructure characteristics in multi-strand aluminum cables (EN AW-1370)−Effect of process parameters [J]. Journal of Manufacturing Processes, 2020, 57: 893−904.
[26] ZHOU L, MIN J, HE W X, HUANG Y X, SONG X G. Effect of welding time on microstructure and mechanical properties of Al−Ti ultrasonic spot welds [J]. Journal of Manufacturing Processes, 2018, 33: 64−73.

超声波焊接铜−铝导线接头的显微组织与力学性能

成先明[1]，杨 可[2]，刘思沾[1]，季珊林[1]，王 健[1]

1. 河海大学 机电工程学院，常州 213022；
2. 河海大学 材料科学与工程学院，常州 213022

摘 要：以 BVR2.5 铜导线和 BLV6.0 铝导线为研究对象，采用不同焊接参数进行超声波焊接。采用 SEM、EDS、数字测温仪、显微硬度计和拉伸试验机研究铜−铝导线接头的显微组织和力学性能。结果表明，当焊接压力为 0.21 MPa、焊接振幅为 31%和焊接时间为 860 ms 时，可以获得拉伸载荷为 355.6 N 的接头。铜/铝相互扩散厚度约 3 μm，焊接峰值温度为 212.2 ℃，没有生成脆硬性的中间相。最佳焊接工艺参数下接头在铜侧断裂，断口为韧−脆混合断裂模式，说明接头性能较好。

关键词：超声波焊接；焊接参数；铜−铝导线接头；显微组织；力学性能

(Edited by Bing YANG)